ACS OMEGA

Article

http://pubs.acs.org/journal/acsodf

Size Effect of Layered Double Hydroxide Platelets on the Crystallization Behavior of Isotactic Polypropylene

Hui Liao, Yingqi Jia, Lumei Wang, Qing Yin, Jingbin Han,* Xiaoli Sun,* and Min Wei

State Key Laboratory of Chemical Resource Engineering, Beijing Advanced Innovation Center for Soft Matter Science and Engineering, Beijing University of Chemical Technology, Beijing 100029, P. R. China

Supporting Information

ABSTRACT: Layered double hydroxide (LDH) platelets with nanosized and microsized level were synthesized and used as fillers in an isotactic polypropylene (PP) matrix. The nucleation and crystallization behavior of PP/LDH composites (denoted as 1-PPL*x* and 2-PPL*x* for composites containing nanosized and microsized LDH, respectively; *x* represents the mass percentage of LDH) was investigated by differential scanning calorimetry and polarized optical microscopy techniques. It is found that the crystallization temperature of PP/LDH composites is largely enhanced and the half crystallization time is reduced remarkably relative to pure PP, especially for 2-PPL*x* composite. The 2-PPL*x* composite exhibits stronger heterogeneous nucleating ability and faster crystallization rate than 1-PPL*x* samples with the same LDH loading. In addition, the crystallized PP/LDH composites possess significantly enhanced thermal stability, gas barrier, and flame-retardant properties relative to neat PP, which would show a broad application prospect in engineering plastics and packing industry.

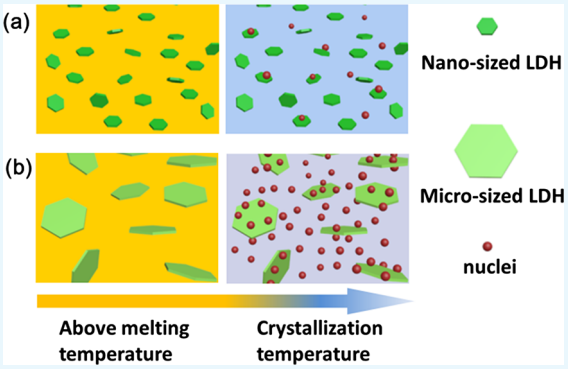

1. INTRODUCTION

Polymer-based composites filled with inorganic compounds have been regarded as one of the most promising materials because the properties of polymers could be improved significantly with the incorporation of inorganic fillers.[1,2] Among the most versatile polymers, polypropylene (PP) is extensively used in industries because of its nontoxicity, corrosion resistance, and good mechanical properties. However, the semicrystalline feature (crystallinity < 60%) of PP normally induces low transparency, long process duration, and poor impact performance, which restricts its application as engineering plastics and transparent packing materials. A large number of inorganic compounds, such as calcium carbonate nanoparticles,[3] carbon nanotubes/fibers,[4] and metal oxides (e.g., TiO_2,[5] SiO_2,[6] and ZnO[7]), have been incorporated into the PP matrix as fillers for better mechanical properties or new functionalities. Recently, lamellar fillers have attracted great interest for preparing PP-based nanocomposites with various unique properties, such as gas barriers and flame-retardant properties.[8−12]

Layered double hydroxide (LDH) is a class of lamellar compounds made up of positively charged brucite-like layers and interlayer charge-compensating anions.[13−16] The flexibility in tuning the composition of both host layers and interlayer anions endows LDH materials with various application prospects in catalysts,[17] biomaterials,[18] and functional additives.[19−21] In particular, LDH is considered as a new emerging class of nanofillers for the preparation of multifunctional polymer/LDH nanocomposites.[22−24] The addition of LDH not only improves the mechanical properties but also endows the polymer/LDH nanocomposites with better properties. For instance, Wang and co-workers[22,25−27] developed a solution blending method to prepare highly dispersed polymer/LDH composites, which exhibit enhanced flame-retardant property and good tunability in rheological behavior. Yan et al.[24] used LDH as a UV-blocking material for improving the thermal stability and photostability of the composites.

For PP/LDH composites, it has been revealed that the incorporation of LDH not only reinforces the physicochemical properties of the composite[28] but also alters the crystallization behavior of PP.[29] It is well-known that the properties of semicrystalline polymers are correlated with their crystalline structure which in turn optimizes their physical properties and processing conditions. The fillers can change the crystallization manner[30] and can tune the structural/morphological characteristics[31,32] of the semicrystalline polymers. Therefore, it is of great importance to investigate the crystallization behavior of polymer/filler composites.[33,34] Although great progress has been achieved on the development of PP/LDH nanocomposites, the crystallization behavior and related crystallization mechanism of the nanocomposites have been rarely reported.[29,35,36] Lonkar and Singh[35] revealed that the

Received: May 17, 2017
Accepted: July 21, 2017
Published: August 4, 2017

DOI: 10.1021/acsomega.7b00621
ACS Omega 2017, 2, 4253−4260

heterogeneous nucleation and crystallization rate of PP were promoted by LDH. Nagendra et al.[29] found that LDH treated by aqueous miscible organic solvent[22] exerts remarkable influence on crystallization kinetics of PP after sonication.

In this work, LDH platelets with different particle sizes were synthesized and applied as inorganic fillers to prepare PP/LDH composites. The crystallization behavior of PP with the assistance of LDH platelets was investigated by differential scanning calorimetry (DSC) and polarized optical microscopy (POM) techniques. A heterogeneous nucleation mechanism is proposed for the PP/LDH composites followed by a three-dimensional (3D) growth of spherocrystals. It is demonstrated that the LDH filler not only accelerated the crystallization rate of PP (especially for microsized LDH) but also enhanced the comprehensive properties of PP/LDH composites.

2. RESULTS AND DISCUSSION

The X-ray diffraction (XRD) patterns (Figure 1a,b) display a well-defined and high-purity LDH phase, with an interlayer spacing of 0.75 nm, corresponding to carbonate LDH. The scanning electron microscopy (SEM) images (Figure 1c,d) show the individual LDH platelets with particle sizes of 200−300 nm and 2−3 μm for the products prepared by the hydrothermal and homogeneous co-precipitation method, respectively. The average diameter is 280 nm and 2.5 μm, revealed by laser grain-size analysis (insets of Figure 1c,d).

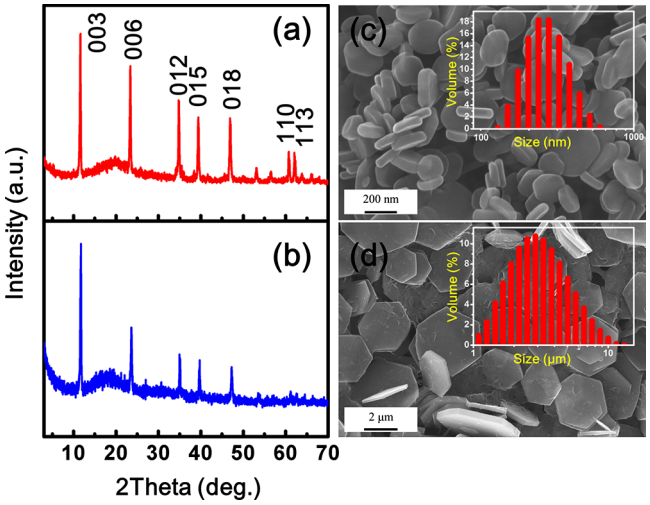

Figure 1. XRD patterns and SEM images of LDH prepared by the (a,c) hydrothermal and (b,d) homogeneous co-precipitation method, respectively. The insets of (b) and (d) illustrate the particle size distribution of the two samples.

The MgAl LDHs prepared below were incorporated with PP using the solution blending method to prepare PP/LDH composites. The composites involving smaller and larger LDH are denoted as 1-PPLx and 2-PPLx, respectively, in which x represents the weight percent of LDH in the composites. The dispersion of an LDH filler in PP/LDH composites (LDH loading = 5%) was observed by transmission electron microscopy (TEM) images (Figure 2), which show that both nanosized and microsized LDH platelets are homogeneously distributed in the PP matrix.

DSC was carried out to explore the crystallization behavior of PP/LDH composites. PP and PP/LDH were first heated from room temperature to 200 °C and held for 3 min to erase the thermal history, then cooled to room temperature at a rate of 10 °C/min to measure the crystallization temperature of pure PP ($T_{c,p}$) and PP/LDH composites ($T_{c,c}$) (Figure 3), and finally reheated to 200 °C at a rate of 10 °C/min to record the melting temperature (T_m) (Figure S1, Supporting Information). It is observed that the crystallization peak temperature of pure PP is located at 112.8 °C, whereas it is enhanced for PP/LDH composites (summarized in Table 1), demonstrating that both LDHs have the effect on inducing PP crystallization. Moreover, the $T_{c,c}$ rises with increasing LDH content, which is indicative of a heterogeneous nucleation mechanism with the presence of LDH. Interestingly, 2-PPLx presents a higher crystallization temperature at equal loading of LDH compared with 1-PPLx.

The difference in crystallization peak temperature between pure PP and PP/filler composites ($\Delta T_c = T_{c,c} - T_{c,p}$) is an important parameter to evaluate the nucleation activity of the nanofiller. It should be noted that the ΔT_c for 2-PPLx composite is among the highest level (summarized in Table S1, Supporting Information), compared with previously reported inorganic nanofillers, illustrating an excellent nucleation activity for microsized LDH. For all the PPLx composites, only one peak is observed at ∼164 °C (melting temperature, T_m) during the melting process, ascribed to the formation of monoclinic α-form PP. Furthermore, the XRD patterns of PP/LDH composites (Figure 4) show a diffraction superposition of LDH and α-PP, where the reflections at 11.8° and 23.7° correspond to the (003) and (006) plane of LDH, respectively, and the other diffraction peaks at 14.2°, 17.0°, 18.7°, 21.3°, and 22.1° are the reflections corresponding to the (110), (040), (130), (111), and (041) crystalline planes of the monoclinic α form of PP, respectively. No other form of PP was induced during the isothermal crystallization process.

To further understand the crystallization behavior of PPLx, the isothermal crystallization of all samples at 135 °C was investigated. A broad crystallization peak of pure PP is

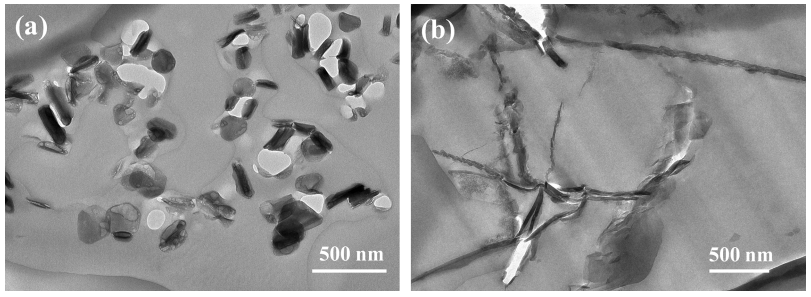

Figure 2. TEM images of PP/LDH composites: (a) 1-PPL5 and (b) 2-PPL5.

DOI: 10.1021/acsomega.7b00621
ACS Omega 2017, 2, 4253−4260

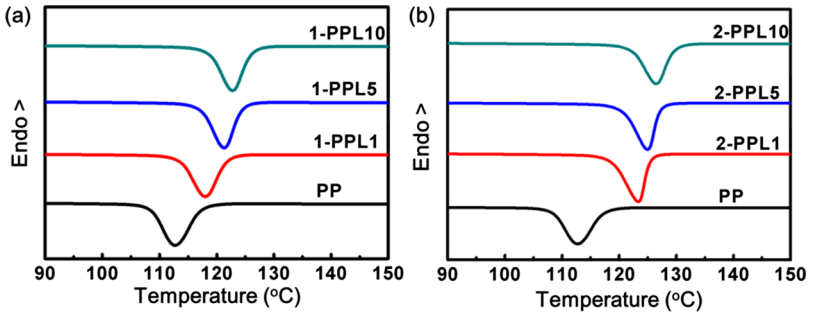

Figure 3. DSC non-isothermal crystallization curves for PP and PP/LDH composites containing (a) nanosized LDH and (b) microsized LDH with a cooling rate of 10 °C/min.

Table 1. Crystallization Peak Temperature of Pure PP ($T_{c,p}$) and PP/LDH Composites ($T_{c,c}$) and Melting Temperature (T_m) of PP and PP/LDH Composites

		composite sample					
temperature/°C	PP	1-PPL1	2-PPL1	1-PPL5	2-PPL5	1-PPL10	2-PPL10
$T_{c,p}$	112.8						
$T_{c,c}$		118.0	123.4	121.3	124.9	122.7	126.5
T_m	161.7	163.7	164.6	163.9	164.7	164.0	164.9

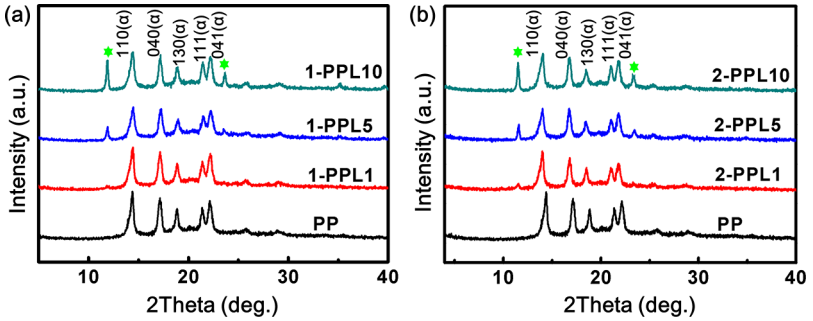

Figure 4. XRD patterns of PP and PP/LDH composites containing (a) nanosized LDH and (b) microsized LDH. Green star represents the diffraction peaks of LDH phase.

presented from ~3 to ~40 min (black line in Figure 5a,b). Upon incorporation with LDH, the peak position undergoes a negative shift accompanied with a narrower peak width as the LDH loading increases, which indicates that the presence of LDH improves the crystallization rate of PP. The relative crystallinity (X_t) was obtained by the integrals at different times (t) divided by the total integral of heat flow (Figure 5c,d). The half crystallization time ($t_{1/2}$), defined as the time when X_t reaches 50%, is a general parameter to inspect the crystallization rate. The $t_{1/2}$ of PP/LDH composites shows a decrease with the increment of LDH loading for both 1-PPLx and 2-PPLx composites (Table 2). In addition, $t_{1/2}$ of 2-PPLx is much smaller than that of 1-PPLx at equal LDH loading, indicative of a higher crystallization rate for 2-PPLx composites.

The following Avrami equation[37] was used to quantitatively elaborate the relationship between LDH content and crystallization kinetics

$$1 - X_t = \exp(-kt^n) \tag{1}$$

where X_t is the relative crystallinity at time t; n is the Avrami exponent relating to the nucleation mechanism and the crystal growth geometry; and k is the crystallization rate constant including both nucleation and growth. In general, the Avrami equation is transformed into a double-logarithmic equation form as follows

$$\ln[-\ln(1 - X_t)] = n \ln t + \ln k \tag{2}$$

The Avrami exponent n was obtained from the slope of the plot for $\ln[-\ln(1 - X_t)]$ versus $\ln t$ (Figure 5e,f) and listed in Table 2. The n value of pure PP is 2.83 and varies from 2.88 to 3.05 for all of these PP/LDH composites. The value of n is close to 3, indicating a typical 3D crystal growth obeying the heterogeneous nucleation mechanism.

The crystallization thermal dynamics and kinetics of PP and its composites containing 5% LDH were further analyzed based on the theory of Hoffman–Lauritzen.[36] The crystallization rate (G), depending on the crystallization temperature (T_c), is expressed as follows

$$G = G_0 \exp\left(-\frac{U^*}{R(T_c - T_\infty)}\right) \exp\left(-\frac{K_g}{T_c \Delta T f}\right) \tag{3}$$

where G_0 is a pre-exponential factor, which is independent of temperature; U^* is the activation energy needed for the chain movement; T_∞ stands for the temperature at which polymer chains are motionless ($T_\infty = T_g - 30$ K, T_g is the glass transition temperature); R is the universal gas constant; ΔT is the undercooling temperature ($\Delta T = T_m^0 - T_c$; T_m^0 is the equilibrium melting temperature); and f is the correction factor, $f = 2T_c/(T_m^0 + T_c)$, in consideration of the fact that the equilibrium melting enthalpy (ΔH_m^0) varies with temperature.

DOI: 10.1021/acsomega.7b00621
ACS Omega 2017, 2, 4253−4260

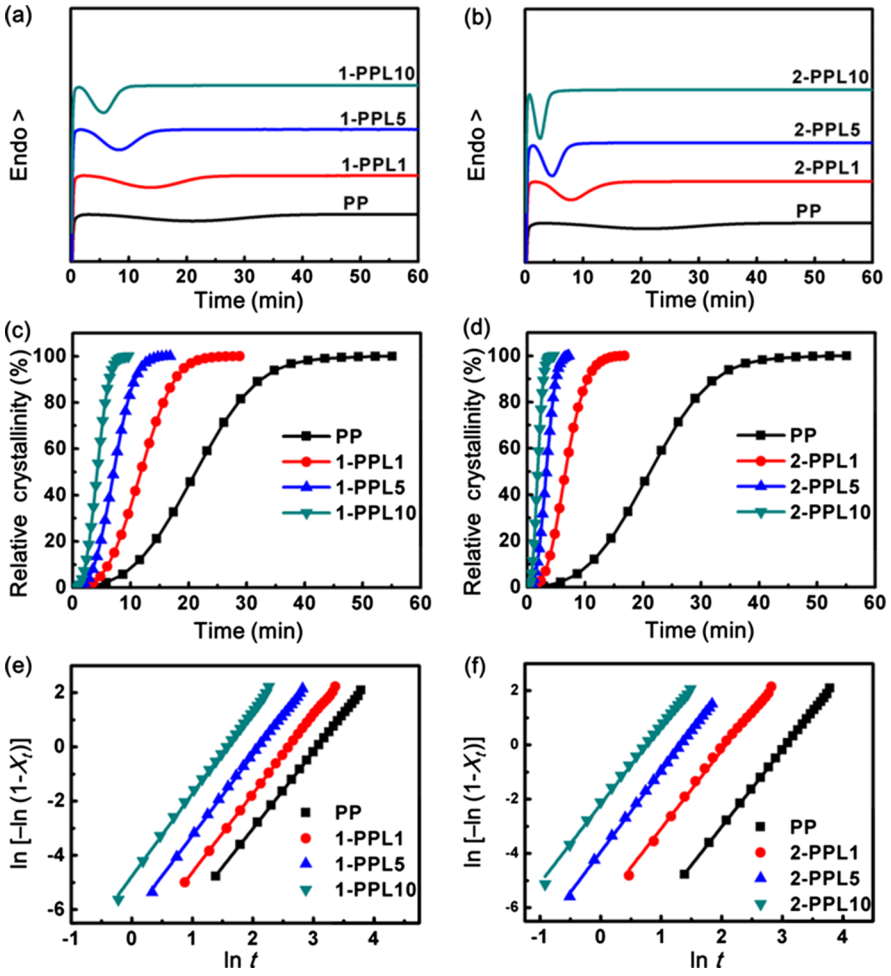

Figure 5. (a,b) DSC curves of isothermal crystallization at 135 °C; (c,d) relative crystallinity as a function of crystallization time t; and (e,f) plots of $\ln[-\ln(1 - X_t)]$ vs ln t for 1-PPLx and 2-PPLx composites.

Table 2. Avrami Exponent and Half Crystallization Time ($t_{1/2}$) of PP and PP/LDH Composites Crystallized at 135 °C

		composite sample					
parameter	PP	1-PPL1	2-PPL1	1-PPL5	2-PPL5	1-PPL10	2-PPL10
n	2.83	2.89	2.88	2.97	2.98	3.05	2.90
$t_{1/2}$/min	18.84	11.82	6.97	7.21	3.32	4.25	1.88

For a heterogeneous nucleation, the nucleation constant K_g can be expressed as follows

$$K_g = \frac{4b_0\sigma\sigma_e T_m^0}{k_B \Delta H_m^0} \quad (4)$$

where b_0 is the distance between two adjacent fold planes; σ and σ_e are the lateral and fold surface free energies, respectively; and k_B is the Boltzmann constant ($k_B = 1.38 \times 10^{-23}$ J K^{-1}). The values of the above-mentioned parameters are listed in Table 3 (obtained from refs 6 38,−41).

The reciprocal of half crystallization time ($1/t_{1/2}$) is approximately equal to the crystallization rate (G). As shown in Figure 6a, all of these samples give a faster crystallization rate in low temperature range, and the microsized LDH promotes PP crystallization at a higher rate under identical conditions. The nucleation constant K_g can be calculated from eq 3, taking the double-logarithmic transformation

$$\ln G + \frac{U^*}{R(T_c - T_\infty)} = \ln G_0 - \frac{K_g}{T_c \Delta T f} \quad (5)$$

The value of G was substituted by $1/t_{1/2}$. Figure S2 (Supporting Information) demonstrates the straight lines based on the plot of $\ln G + U^*/R(T_c - T_\infty)$ versus $1/T_c\Delta Tf$. The value of K_g can be obtained from the slope of the straight lines (summarized in Table 4).

The fold surface free energy (σ_e) is an important parameter to evaluate the nucleating effect of a nanofiller, that is, a nanofiller with high nucleating ability can reduce σ_e.[42] The σ_e of PP, 1-PPL5, and 2-PPL5 was calculated (through eq 4) to be 0.198, 0.177, and 0.159 J m^{-2} (Table 4), respectively, in

Table 3. Values for the Parameters in Eqs 3 and 4

U^* (J K^{-1})	T_g (K)	T_∞ (K)	T_m^0 (°C)	b_0 (Å)	σ (J m^{-2})	ΔH_m^0 (J m^{-3})
6300	270	240	212.1	6.26	1.10×10^{-2}	1.93×10^8

DOI: 10.1021/acsomega.7b00621
ACS Omega 2017, 2, 4253−4260

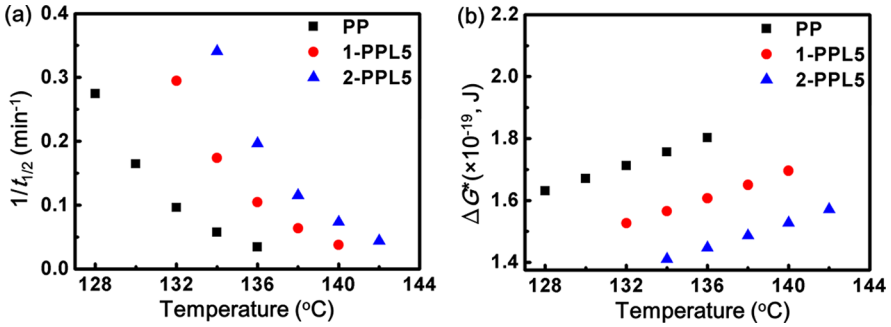

Figure 6. Crystallization kinetics of PP, 1-PPL5, and 2-PPL5 at different temperatures: (a) plots of $1/t_{1/2}$ vs temperature and (b) plots of the free energy of nucleation (ΔG^*) vs crystallization temperature.

Table 4. Kinetic Parameter (K_g) and Fold Surface Free Energy (σ_e) of PP, 1-PPL5, and 2-PPL5

Parameter	PP	1-PPL5	2-PPL5
K_g (10^5 K^2)	9.94	8.86	7.98
σ_e (J m^{-2})	0.198	0.177	0.159

accordance with the superior ability of microsized LDH toward PP nucleation.

The free energy (ΔG^*) necessary for the formation of a nucleus with critical size was calculated by the following equation

$$\Delta G^* = \frac{4b_0\sigma\sigma_e T_m^0}{\Delta H_m^0 \Delta T} \quad (6)$$

As shown in Figure 6b, for these samples, ΔG^* increases as the temperature rises, and the incorporation of LDH decreases the energy barrier for the nucleation of PP/LDH composites. Similar result was also observed in other PP/inorganic filler systems (e.g., MoS_2/PP composite).[43] Significantly, the ΔG^* of 2-PPL5 is lower than that of 1-PPL5 at the same crystallization temperature. This result indicates that LDH reduces the free energy of nucleation and the microsized LDH shows a better performance. Therefore, the overall crystallization rate is improved markedly by LDH, especially for microsized LDH.

It is well-known that the crystallization morphology of PP is greatly affected by the fillers. The POM images (Figure 7) display common spherulitic structure with well-defined boundaries (spherulite size: ~70 μm) for pristine PP after isothermal crystallization. However, the spherulitic structure of PP/LDH composites is not as perfect as neat PP with much smaller spherulite size, which is attributed to the enhanced crystallization rate. For 1-PPL*x* composites, the samples with 1 and 5% LDH loading still present spherulitic structure with smaller size, whereas no defined spherulites are discovered in the field of vision with a further increase of LDH loading. The 2-PPL*x* composites show a similar variation in the crystal structure, but only 2-PPL1 sample maintains perfect spherulites. No defined spherulite is observed for 2-PPL5 and 2-PPL10 composites.

The variety of crystallization morphology of 1-PPL5 and 2-PPL5 with different crystallization times was further recorded by in situ POM. For 1-PPL5 composite, only a few small crystals appear randomly at 5 min (Figure 8a). The crystals grow gradually in size, form into spherulites with clear boundaries (Figure 8b–d), and then terminate at 30 min as a result of the spherulite collision. In the case of 2-PPL5 composite, the density of nuclei is much higher than that of 1-PPL5; numerous tiny crystals emerge at 2.5 min (Figure 8e). The crystals keep growing into a bigger imperfect spherulite, which is accomplished within 15 min approximately (Figure 8e–h). It is thus concluded that the presence of LDH particles provides heterogeneous nuclei for PP crystallization, leading to the increase of spherulite density and decrease of spherulite size. In comparison with nanosized LDH, the microsized LDH induces more nuclei in the PP matrix and thus exhibits a stronger heterogeneous nucleating ability. The precise epitaxial mechanism of PP on LDH is still under working.

The size of LDH not only affects the heterogeneous nucleating ability but also impacts the thermal conductive property of the composites, which consequently plays a key role

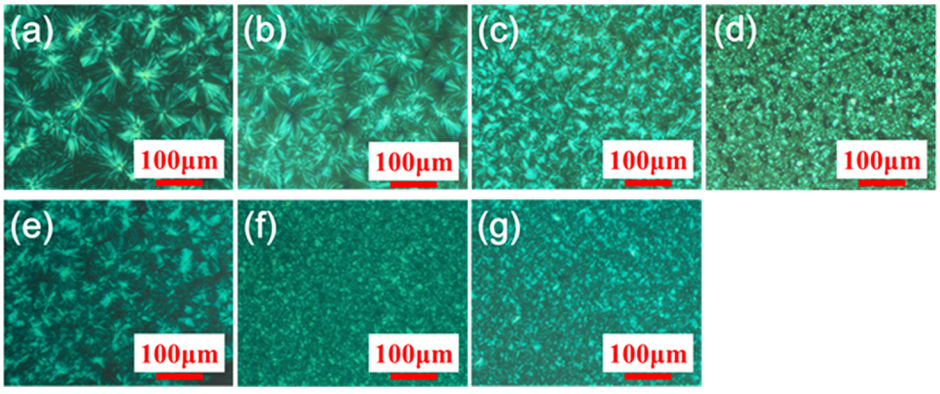

Figure 7. POM images of PP and PP/LDH composites crystallized isothermally at 135 °C: (a) PP, (b) 1-PPL1, (c) 1-PPL5, (d) 1-PPL10, (e) 2-PPL1, (f) 2-PPL5, and (g) 2-PPL10.

DOI: 10.1021/acsomega.7b00621
ACS Omega 2017, 2, 4253–4260

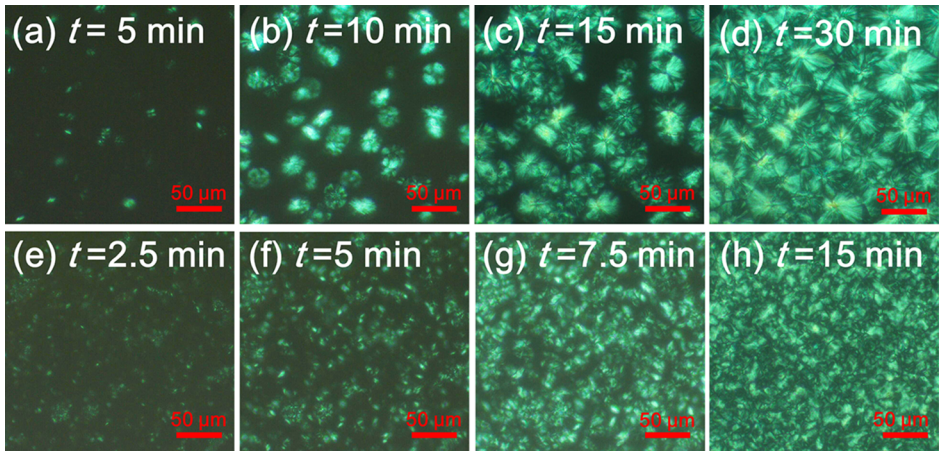

Figure 8. In situ POM images of (a–d) 1-PPL5 and (e–h) 2-PPL5 composites at various crystallization times.

on the crystallization behavior of polymer/filler composites.[44] The thermal diffusivity and specific heat capacity of two kinds of LDH were measured by a laser flash thermal conductivity analyzer and DSC. The thermal conductivity (λ) is calculated by the equation $\lambda = C_p \times \rho \times a$, where C_p is the specific heat capacity; ρ is the density of circular plate samples; and a is the thermal diffusivity. As shown in Table 5, the thermal conductivity of microsized LDH is 1.39 W m^{-1} K^{-1}, which is much larger than that of nanosized LDH (0.85 W m^{-1} K^{-1}). The higher thermal conductivity of microsized LDH enables the temperature of the PP/microsized LDH composite to drop faster, when cooling from the melting temperature to the crystallization temperature. In case the temperature at the LDH/PP interface is lower than the critical condition, the nucleation will occur first on the LDH surface (as shown in Scheme 1), and then the crystals grow gradually and form into spherulites. Therefore, the PP composites filled by microsized LDH show a faster crystallization rate than the PP/nanosized LDH composites.

Table 5. Thermal Diffusivity (a), Specific Heat Capacity (C_p), and Thermal Conductivity (λ) for Nanosized and Microsized LDH

parameter	nanosized LDH	microsized LDH
a (mm^2 s^{-1})	0.30	0.22
C_p (J g^{-1} K^{-1})	1.99	4.65
λ (W m^{-1} K^{-1})	0.85	1.39

Scheme 1. Schematic Diagram of the Nucleation in (a) 1-PPL*x* and (b) 2-PPL*x* Composites

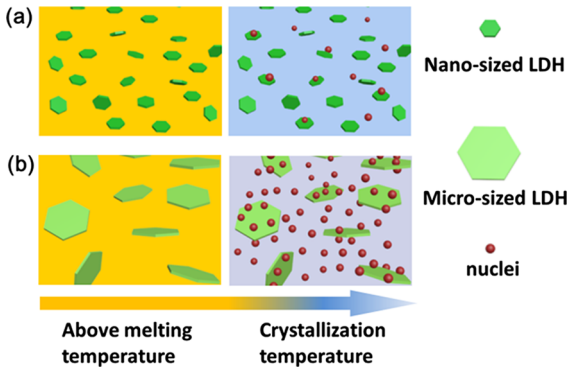

The influence of LDH on the thermal stability of PP/LDH composites was investigated using thermal gravimetric analysis (TGA) (Figure 9). All of these PP/LDH composites display enhanced thermal stability than pristine PP judged from the 50% weight loss temperature ($T_{0.5}$) (summarized in Table 6). Interestingly, 1-PPL*x* represents better thermal stability compared with 2-PPL*x* with equal loading of LDH.

The flammability study (see details in the Supporting Information, Figure S3 and Table S2) reveals that nanosized LDH has a better effect on the flame retardancy of PP/LDH composites. The superior thermal stability and flame-retardant property of 1-PPL*x* are ascribed to the lower thermal conductivity of nanosized LDH, which hinders the heat transport throughout the composite. In addition, the gas permeability property of PP/LDH composites was also studied (Figure S4, Supporting Information); an inhibited oxygen transmission rate of PP/LDH composites was found compared with neat PP, and 2-PPL*x* exhibits superior gas barrier behavior than 1-PPL*x* because of the larger LDH platelet size and higher spherulite density.

3. CONCLUSIONS

In summary, nanosized LDH and microsized LDH were incorporated with isotactic PP by a solution blending method. The nucleation and crystallization behavior of PP/LDH composites with various LDH loadings was investigated by DSC and POM techniques. As the LDH loading increases, the spherulite density of α-PP becomes larger and the spherulite size is significantly reduced. A particle-size-dependent crystallization property is observed for PP/LDH composites: the microsized LDH provides more nuclei and shows stronger heterogeneous nucleation ability for PP crystallization, resulting in a faster crystallization rate. Several physical properties, including thermal stability, gas barrier property, and flame retardancy, are improved greatly after incorporation of the LDH filler. The crystallized PP/LDH composites have broad applications in building materials, medical devices, and packaging products.

4. EXPERIMENTAL SECTION

4.1. Reagents and Materials. The isotactic PP with melt flow index of 2.2 was purchased from Shanghai Aladdin Reagent Co. Ltd. $Mg(NO_3)_2{\cdot}6H_2O$, $Al(NO_3)_3{\cdot}9H_2O$, NaOH,

DOI: 10.1021/acsomega.7b00621
ACS Omega 2017, 2, 4253–4260

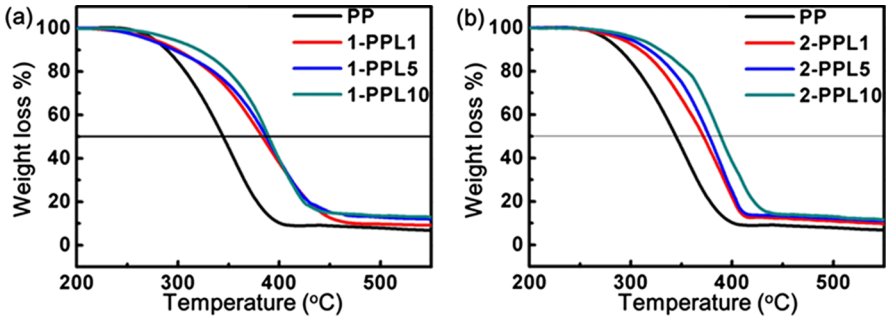

Figure 9. TGA for (a) 1-PPL*x* and (b) 2-PPL*x* composites.

Table 6. 50% Weight Loss Temperature ($T_{0.5}$) for PP and PP/LDH Composites

		PPL1		PPL5		PPL10	
	PP	1-PPL1	2-PPL1	1-PPL5	2-PPL5	1-PPL10	2-PPL10
$T_{0.5}$/°C	345	398	372	396	377	390	389

Na_2CO_3, urea, ethanol, and acetone were analytical grade chemicals and used without further purification.

4.2. Preparation of MgAl LDHs with Different Particle Sizes. The hydrothermal method was used to prepare nanosized MgAl LDH. A 50 mL of mixed metal salt solution containing 0.025 mol $Mg(NO_3)_2{\cdot}6H_2O$ and 0.0125 mol $Al(NO_3)_3{\cdot}9H_2O$ was added dropwise into a Na_2CO_3 solution (0.5 mol/L, 50 mL) with continuous stirring. The pH of the reaction solution was controlled at ∼10 using a 2 mol/L NaOH solution. Finally, the suspension was transferred into an autoclave and placed into an oven at 150 °C for 24 h.

The microsized LDH was prepared by a homogeneous coprecipitation method using urea as the alkali resource. $Mg(NO_3)_2{\cdot}6H_2O$, $Al(NO_3)_3{\cdot}9H_2O$, and urea were dissolved in deionized water with concentrations of 0.08, 0.04, and 0.48 mol/L, respectively. The mixture was aged in a three-neck round-bottom flask equipped with a reflux condenser at 100 °C under continuous stirring for 24 h.

Both of these products were washed with deionized water until the pH value reached to 7.0, followed by separation by a centrifuge (4000 rpm). Subsequently, the LDH product was washed three times using ethanol and then washed with acetone for another three times. The resulting LDH sample was directly used for the preparation of PP/LDH composites.

4.3. Preparation of PP/LDH Composites. The solution blending method developed by Wang et al.[22] was used to prepare a series of PP/LDH composites (LDH content = 1, 5, and 10% by weight). PP (5 g) was dissolved into xylene (25 mL) in a round-bottle flask with a reflux condenser in a nitrogen atmosphere at 150 °C. After PP was completely dissolved, another 25 mL of xylene containing different weight percent of MgAl LDH was added. The mixed solution was continuously stirred for 24 h and poured into 50 mL of ethanol. The precipitation was filtered and washed thoroughly with ethanol to remove the residual xylene. Finally, the product was dried in a vacuum oven at 60 °C for 24 h.

■ ASSOCIATED CONTENT

Supporting Information

The Supporting Information is available free of charge on the ACS Publications website at DOI: 10.1021/acsomega.7b00621. Characterization techniques; the melting curves; the plots of ln $G + U^*/R(T_c - T_\infty)$ versus $1/T_c\Delta Tf$; the plots of HRR versus temperature; oxygen transmission rate; comparison of the crystallization peak temperature between PP/LDH (this work) composites and previous report; and heat release capacity (HRC), peak of heat release rate (PHRR), and total heat release (THR) (PDF)

■ AUTHOR INFORMATION

Corresponding Authors

*E-mail: hanjb@mail.buct.edu.cn. Phone: +86-10-64412131. Fax: +86-10-64425385 (J.H.).
*E-mail: xiaolisun@mail.buct.edu.cn (X.S.).

ORCID

Min Wei: 0000-0001-7540-0824

Notes

The authors declare no competing financial interest.

■ ACKNOWLEDGMENTS

This work was supported by the 973 Program (grant no. 2014CB932102), the National Natural Science Foundation of China (NSFC), and the Beijing Nova Program.

■ REFERENCES

(1) Cho, E. S.; Coates, N. E.; Forster, J. D.; Ruminski, A. M.; Russ, B.; Sahu, A.; Su, N. C.; Yang, F.; Urban, J. J. Engineering synergy: Energy and mass transport in hybrid nanomaterials. *Adv. Mater.* **2015**, *27*, 5744−5752.

(2) Bitinis, N.; Hernandez, M.; Verdejo, R.; Kenny, J. M.; Lopez-Manchado, M. A. Recent advances in clay/polymer nanocomposites. *Adv. Mater.* **2011**, *23*, 5229−5236.

(3) Chan, C.-M.; Wu, J.; Li, J.-X.; Cheung, Y.-K. Polypropylene/calcium carbonate nanocomposites. *Polymer* **2002**, *43*, 2981−2992.

(4) Cao, L.; Su, D.; Su, Z.; Chen, X. Fabrication of multiwalled carbon nanotube/polypropylene conductive fibrous membranes by melt electrospinning. *Ind. Eng. Chem. Res.* **2014**, *53*, 2308−2317.

(5) Altan, M.; Yildirim, H. Mechanical and antibacterial properties of injection molded polypropylene/TiO_2 nano-composites: effects of surface modification. *J. Mater. Sci. Technol.* **2012**, *28*, 686−692.

(6) Papageorgiou, G. Z.; Achilias, D. S.; Bikiaris, D. N.; Karayannidis, G. P. Crystallization kinetics and nucleation activity of filler in polypropylene/surface-treated SiO_2 nanocomposites. *Thermochim. Acta* **2005**, *427*, 117−128.

(7) Zhao, H.; Li, R. K. Y. A study on the photo-degradation of zinc oxide (ZnO) filled polypropylene nanocomposites. *Polymer* **2006**, *47*, 3207−3217.

(8) Kim, B.; Lee, S.-H.; Lee, D.; Ha, B.; Park, J.; Char, K. Crystallization kinetics of maleated polypropylene/clay hybrids. *Ind. Eng. Chem. Res.* **2004**, *43*, 6082−6089.

DOI: 10.1021/acsomega.7b00621
ACS Omega 2017, 2, 4253−4260

(9) Hofmann, D.; Wartig, K.-A.; Thomann, R.; Dittrich, B.; Schartel, B.; Mülhaupt, R. Functionalized graphene and carbon materials as additives for melt-extruded flame retardant polypropylene. *Macromol. Mater. Eng.* **2013**, *298*, 1322−1334.
(10) Yu, B.; Wang, X.; Qian, X.; Xing, W.; Yang, H.; Ma, L.; Lin, Y.; Jiang, S.; Song, L.; Hu, Y.; Lo, S. Functionalized graphene oxide/phosphoramide oligomer hybrids flame retardant prepared via in situ polymerization for improving the fire safety of polypropylene. *RSC Adv.* **2014**, *4*, 31782−31794.
(11) Lonkar, S. P.; Therias, S.; Leroux, F.; Gardette, J. L.; Singh, R. P. Influence of reactive compatibilization on the structure and properties of PP/LDH nanocomposites. *Polym. Int.* **2011**, *60*, 1688−1696.
(12) Qiu, L.; Gao, Y.; Yan, X.; Guo, J.; Umar, A.; Guo, Z.; Wang, Q. Morphology-dependent performance of Mg_3Al-CO_3 layered double hydroxide as a nanofiller for polypropylene nanocomposites. *RSC Adv.* **2015**, *5*, 51900−51911.
(13) Wang, Q.; O'Hare, D. Recent Advances in the Synthesis and Application of Layered Double Hydroxide (LDH) Nanosheets. *Chem. Rev.* **2012**, *112*, 4124−4155.
(14) Gu, Z.; Atherton, J. J.; Xu, Z. P. Hierarchical layered double hydroxide nanocomposites: structure, synthesis and applications. *Chem. Commun.* **2015**, *51*, 3024−3036.
(15) Zhao, M.-Q.; Zhang, Q.; Huang, J.-Q.; Wei, F. Hierarchical nanocomposites derived from nanocarbons and layered double hydroxides - properties, synthesis, and applications. *Adv. Funct. Mater.* **2012**, *22*, 675−694.
(16) Yan, D.; Lu, J.; Duan, X. Recent advance in structure and interaction study on layered double hydroxide. *Sci. China: Chem.* **2013**, *43*, 1135−1148.
(17) Wang, J.; Fan, G.; Wang, H.; Li, F. Synthesis, characterization, and catalytic performance of highly dispersed supported nickel catalysts from Ni−Al layered double hydroxides. *Ind. Eng. Chem. Res.* **2011**, *50*, 13717−13726.
(18) Du, N.; Hou, W.-G.; Song, S.-E. A novel composite: layered double hydroxides encapsulated in vesicles. *J. Phys. Chem. B* **2007**, *111*, 13909−13913.
(19) Lei, X.; Jin, M.; Williams, G. R. Layered double hydroxides in the remediation and prevention of water pollution. *Energy Environ. Focus* **2014**, *3*, 4−22.
(20) Wang, P.-J.; Hu, X.-P.; Liao, D.-J.; Wen, Y.; Hull, T. R.; Miao, F.; Zhang, Q.-T. Dual fire retardant action: the combined gas and condensed phase effects of azo-modified NiZnAl layered double hydroxide on intumescent polypropylene. *Ind. Eng. Chem. Res.* **2017**, *56*, 920−932.
(21) Feng, Y.; Jiang, Y.; Huang, Q.; Chen, S.; Zhang, F.; Tang, P.; Li, D. High antioxidative performance of layered double hydroxides/polypropylene composite with intercalation of low-molecular-weight phenolic antioxidant. *Ind. Eng. Chem. Res.* **2014**, *53*, 2287−2292.
(22) Wang, Q.; Zhang, X.; Zhu, J.; Guo, Z.; O'Hare, D. Preparation of stable dispersions of layered double hydroxides (LDHs) in nonpolar hydrocarbons: new routes to polyolefin/LDH nanocomposites. *Chem. Commun.* **2012**, *48*, 7450−7452.
(23) Zhang, H.; Zhang, J.; Yun, R.; Jiang, Z.; Liu, H.; Yan, D. Nanohybrids of organo-modified layered double hydroxides and polyurethanes with enhanced mechanical, damping and UV absorption properties. *RSC Adv.* **2016**, *6*, 34288−34296.
(24) Wang, G.; Xu, S.; Xia, C.; Yan, D.; Lin, Y.; Wei, M. Fabrication of host−guest UV-blocking materials by intercalation of fluorescent anions into layered double hydroxides. *RSC Adv.* **2015**, *5*, 23708−23714.
(25) Wang, Q.; Zhang, X.; Wang, C. J.; Zhu, J.; Guo, Z.; O'Hare, D. Polypropylene/layered double hydroxide nanocomposites. *J. Mater. Chem.* **2012**, *22*, 19113−19121.
(26) Wang, Q.; O'Hare, D. Large-scale synthesis of highly dispersed layered double hydroxide powders containing delaminated single layer nanosheets. *Chem. Commun.* **2013**, *49*, 6301−6303.
(27) Gao, Y.; Wu, J.; Wang, Q.; Wilkie, C. A.; O'Hare, D. Flame retardant polymer/layered double hydroxide nanocomposites. *J. Mater. Chem. A* **2014**, *2*, 10996−11016.
(28) Nagendra, B.; Rosely, C. V. S.; Leuteritz, A.; Reuter, U.; Gowd, E. B. Polypropylene/layered double hydroxide nanocomposites: influence of LDH intralayer metal constituents on the properties of polypropylene. *ACS Omega* **2017**, *2*, 20−31.
(29) Nagendra, B.; Mohan, K.; Gowd, E. B. Polypropylene/layered double hydroxide (LDH) nanocomposites: influence of LDH particle size on the crystallization behavior of polypropylene. *ACS Appl. Mater. Interfaces* **2015**, *7*, 12399−12410.
(30) Li, S.; Auddy, K.; Barber, P.; Hansen, T. J.; Ma, J.; zur Loye, H.-C.; Ploehn, H. J. Thermal, mechanical, and barrier properties of polyethylene terephthalate-platelet nanocomposites prepared by in situ polymerization. *Polym. Eng. Sci.* **2012**, *52*, 1888−1902.
(31) Li, L.; Li, B.; Hood, M. A.; Li, C. Y. Carbon nanotube induced polymer crystallization: The formation of nanohybrid shish−kebabs. *Polymer* **2009**, *50*, 953−965.
(32) Laird, E. D.; Li, C. Y. Structure and morphology control in crystalline polymer−carbon nanotube nanocomposites. *Macromolecules* **2013**, *46*, 2877−2891.
(33) Ning, N.; Fu, S.; Zhang, W.; Chen, F.; Wang, K.; Deng, H.; Zhang, Q.; Fu, Q. Realizing the enhancement of interfacial interaction in semicrystalline polymer/filler composites via interfacial crystallization. *Prog. Polym. Sci.* **2012**, *37*, 1425−1455.
(34) Li, H.; Yan, S. Surface-induced polymer crystallization and the resultant structures and morphologies. *Macromolecules* **2011**, *44*, 417−428.
(35) Lonkar, S. P.; Singh, R. P. Isothermal crystallization and melting behavior of polypropylene/layered double hydroxide nanocomposites. *Thermochim. Acta* **2009**, *491*, 63−70.
(36) Yang, H.; Liu, J.; Zhou, X.; Diao, M.; Qiu, X.; Yang, C.; Qin, J. Isothermal crystallization kinetics of layered double hydroxides/β nucleating agent modified isotactic polypropylene. *Eng. Plast. Appl.* **2014**, *42*, 93−97, DOI: 10.3969/j.issn.1001-3539.2014.01.020.
(37) Avrami, M. Kinetics of phase change. I general theory. *J. Chem. Phys.* **1939**, *7*, 1103−1112.
(38) Hoffman, J. D.; Miller, R. L. Kinetic of crystallization from the melt and chain folding in polyethylene fractions revisited: theory and experiment. *Polymer* **1997**, *38*, 3151−3212.
(39) Clark, E. J.; Hoffman, J. D. Regime III crystallization in polypropylene. *Macromolecules* **1984**, *17*, 878−885.
(40) Lu, X. F.; Hay, J. N. Isothermal crystallization kinetics and melting behaviour of poly(ethylene terephthalate). *Polymer* **2001**, *42*, 9423−9431.
(41) Xu, J.; Srinivas, S.; Marand, H.; Agarwal, P. Equilibrium melting temperature and undercooling dependence of the spherulitic growth rate of isotactic polypropylene. *Macromolecules* **1998**, *31*, 8230−8242.
(42) Marco, C.; Naffakh, M.; Gómez, M. A.; Santoro, G.; Ellis, G. The crystallization of polypropylene in multiwall carbon nanotube-based composites. *Polym. Compos.* **2011**, *32*, 324−333.
(43) Naffakh, M.; Marco, C.; Gómez-Fatou, M. A. Isothermal crystallization kinetics of novel isotactic polypropylene/MoS_2 inorganic nanotube nanocomposites. *J. Phys. Chem. B* **2011**, *115*, 2248−2255.
(44) Cai, Y.; Petermann, J.; Wittich, H. Transcrystallization in fiber-reinforced isotactic polypropylene composites in a temperature gradient. *J. Appl. Polym. Sci.* **1997**, *65*, 67−75.

DOI: 10.1021/acsomega.7b00621
ACS Omega 2017, 2, 4253−4260